Full Length Article

# Improving the biodiesel combustion and emission characteristics in the lean pre-vaporized premixed system using diethyl ether as a fuel additive

Radwan M. EL-Zohairy [1], Ahmed S. Attia [1], A.S. Huzayyin, Ahmed I. EL-Seesy [*]

*Mechanical Engineering Department, Benha, Benha Faculty of Engineering, Benha University, 13512 Benha, Qalubia, Egypt*

## ARTICLE INFO

## ABSTRACT

This paper is a lab-scale experimental study of the impact of employing diethyl ether (DEE) as an additive to waste cooking oil biodiesel with Jet A-1 on the combustion as well as emission features of a swirl-stabilized premixed flame. First, waste cooking oil biodiesel with a volume fraction of 20% was blended with Jet A-1 and symbolized as W20. Then, diethyl ether with a volume fraction of 20% was blended with 20% biodiesel and 60% Jet A-1, symbolized as W20D20. The three test fuels (W20, W20D20 blend, and pure Jet A-1) were premixed with preheated air and pre-vaporized before being admitted to the vertical cylindrical combustor having an inner diameter of 150 mm and a length of 500 mm via a swirl burner (radial type) of 0.55 swirl number and 8 straight vanes with an angle of 45°. Local flame temperatures and emissions were measured and recorded at 350 °C of preheated air with a constant equivalence ratio ($\varphi$) of 0.85. According to the findings, a relatively wide range of flame temperatures was observed in the flame of the W20 blend, while the W20D20 blend had a flame temperature distribution very close to that of the Jet A-1. The W20D20 blend reduced UHC emissions by 69.6%, CO emissions by 61.4%, and $NO_x$ emissions by 12.5% relative to Jet A-1 at the combustion chamber outlet. Overall, adding DEE to biodiesel significantly impacts both combustion and emission profiles.

## 1. Introduction

The world faces a crisis in energy demand and environmental threats from emission levels and greenhouse gases, which cause global warming [1]. In particular, aircraft engines are responsible for about 3% of global warming emissions, and it is expected that they will increase their future contribution [2]. Because of these environmental risks and the lack of fossil fuels, there is a growing interest in renewable alternatives to aviation fuels [2]. In recent years, biodiesel has gained significant attention because it has many attractive features (renewable, biodegradable, and non-toxic) [3]. In addition, biodiesel has the potential to significantly reduce emissions of dangerous pollutants like nitrogen oxides ($NO_x$), carbon monoxide (CO), and unburned hydrocarbons (UHC) [1]. Habib et al. [4] proved that biodiesel fuels made from recycled rapeseed, soybeans, canola oil, and hog fat resulted in lower CO and $NO_x$ emissions than using Jet A-1 in gas turbines.

One of the important sources for biodiesel production is waste cooking oil. The world produces annually large quantities of waste cooking oil. Table 1 lists the availability of waste cooking oil in different countries. Egypt produces annually a half-million tons of waste cooking

oil of food factories, hotels, restaurants, and homes [5]. Around 90% of homes pour leftover cooking oil into drains, which means that it cannot be reused. Waste oil collection systems have not yet been established effectively, even in large cities [6]. This large quantity of waste oil cannot be ignored, as it could be a leading feedstock for biodiesel production. So, waste cooking oil should be recycled into biodiesel rather than polluting the environment. Recycling used oil for producing biodiesel was first proposed in Egypt in 2013 [5]. Gas turbines produce a steady flame during combustion, this advantage allows gas turbines to burn varied fuels like biodiesel cleanly [7]. Also, in a radial swirler gas turbine combustor, Li et al. [8] found that using WCO biodiesel reduced CO, $NO_x$, and UHC emissions in the lean combustion range.

Unlike diesel, biodiesel still has a number of undesired properties, including higher surface tension, viscosity, and reduced volatility [9]. Additionally, biodiesel can not be sprayed or atomized to the same degree as diesel [10]. This could result in inadequate efficiency in creating a flammable mixture [10]. Wang et al. and Agarwal & Chaudhury [11,12] evaluated biodiesel-diesel spray properties and found that it had a longer spray tip penetration (STP), decreased air mixing, and a larger Sauter Mean Diameter (SMD), that weakens mixture formation. These limitations explain why biodiesel is rarely used in concentrations higher

**Nomenclature**

| | |
|---|---|
| CO | Carbon monoxide |
| $CO_2$ | Carbon dioxide |
| $NO_x$ | Nitrogen oxides |
| UHC | Unburned hydrocarbons |
| SMD | Sauter mean diameter |
| DEE | Diethyl ether |
| DBE | Dibutyl ether |
| LPP | Lean pre-vaporized premixed |
| WCO | Waste cooking oil |
| WCOME | Waste cooking oil methyl ester |
| STP | Spray tip penetration |
| SCA | Spray cone angle |
| SPA | Spray projected area |
| KOH | Potassium hydroxide |
| SN | Swirl number |
| CN | Cetane number |
| $W_{20}$ | Blend contains 20% biodiesel and 80% Jet A-1 by volume |
| $W_{20}D_{20}$ | Blend contains 20% DEE, 20% biodiesel, and 60 % Jet A-1 |
| TGA | Thermogravimetric analysis |
| LHV | Lower heating value |
| EA | Elemental analyzer |
| $A/F_{stio}$ | Stoichiometric air–fuel ratio |
| $\varphi$ | Equivalence ratio |
| $\dot{m}_a$ | Air flow rate |
| $\dot{m}_f$ | Fuel flow rate |
| $\sigma$ | Surface tension |
| $\mu$ | Dynamic viscosity |
| PF | Pattern factor |
| $T_{max}$ | Maximum recorded temperature |
| $T_{mean}$ | Mean outlet temperature |
| $T_{in}$ | Incoming air temperature |
| $T_f$ | Flame temperature (K) |
| FTD | Flame temperature distribution |
| IR | Infrared |
| Z | Vertical distance from the burner tip (mm) |
| R | Radial distance from the burner centerline (mm) |

**Table 1**

WCO availability in some countries [6].

| Country | (Million tons of WCO/year) |
|---|---|
| China | 6.580 |
| Egypt | 0.5 |
| USA | 1.4 |
| Japan | 0.4 |
| EU | 1 |
| South Africa | 0.2 |

than 20% when blended with diesel. It is proposed that biodiesel's poor cold flow properties can be improved by blending it with a less viscous fuel, such as diethyl ether (DEE), to reduce the fuel viscosity, surface tension, and density [13]. Additionally, DEE is an oxygenated additive, and blended with biodiesel can help reduce exhaust emissions even more [1].

One promising biofuel is (DEE $(C_2H_5)_2O$), which can be produced by ethanol dehydration utilizing solid acid catalysts [14]. DEE is ideal for engine starting, especially at low temperatures, due to its high vapor pressure, which enhances the atomization and mixture formation process [15]. Additionally, compared to diesel and biodiesel, DEE has a larger latent heat of evaporation. In this way, the maximum temperature of the combustion can be lowered by blending DEE with diesel or

**Table 2**

Previous studies of using ether fuels as additives.

| Reference | Base Fuel | Additive | Mixing ratio | Combustion mode | Parameters studied | Results |
|---|---|---|---|---|---|---|
| [13] | Diesel (D) | Soybean Biodiesel (B) Di-n-butyl Ether (E) | • D100 B100 B85E15 B70E30 | spray combustion | SCA, STP, and SPA | • The blends' STP was shortened. A larger SCA was adopted. |
| [10] | Diesel (D) | soybean biodiesel (B), ethanol (E), diethyl ether (DEE) | • D100 D80B20 D64B16E20 D64B16DEE20 | spray combustion | STP, SCA, and SMD | • Biodiesel increased SMD. DEE decreased SMD. DEE improved the degree of atomization. |
| [17] | dimethyl ether | _ | _ | Co-flow burner | The flame structure, liftoff behavior | • The liftoff altitudes rose linearly with the increase of central jet flow. The liftoff altitude and the CH4 equivalence ratio were negatively related. |
| [16] | Methyl decanoate (MD) | The dibutyl ether (DBE). | • MD100 DBE10 DBE20 DBE30 DBE40 | Co-flow diffusion burner | Soot production and particle emission. | • DBE decreased soot formation. |
| [18] | Diesel (D) | Soybean biodiesel (B), n-butyl ether (DBE). | • Diesel B100 DBE100 DBE15 DBE30 | spray combustion | STP, SCA, SPA, SMD | • Biodiesel had lower SCA and SPA than blended fuels. The spray of biodiesel had a high tendency to larger SMD, while DBE30 spray has smaller SMD. Biodiesel atomization was greatly enhanced by DBE. |
| [19] | Diesel (D) | dimethyl ether (DME) | • D100 DME5 by weight DME10 DME100 | spray combustion | Spray shape, SCA, STP | • SCA increased with increased DME blending ratios. Increased DME mixing ratio resulted in a shorter STP. |
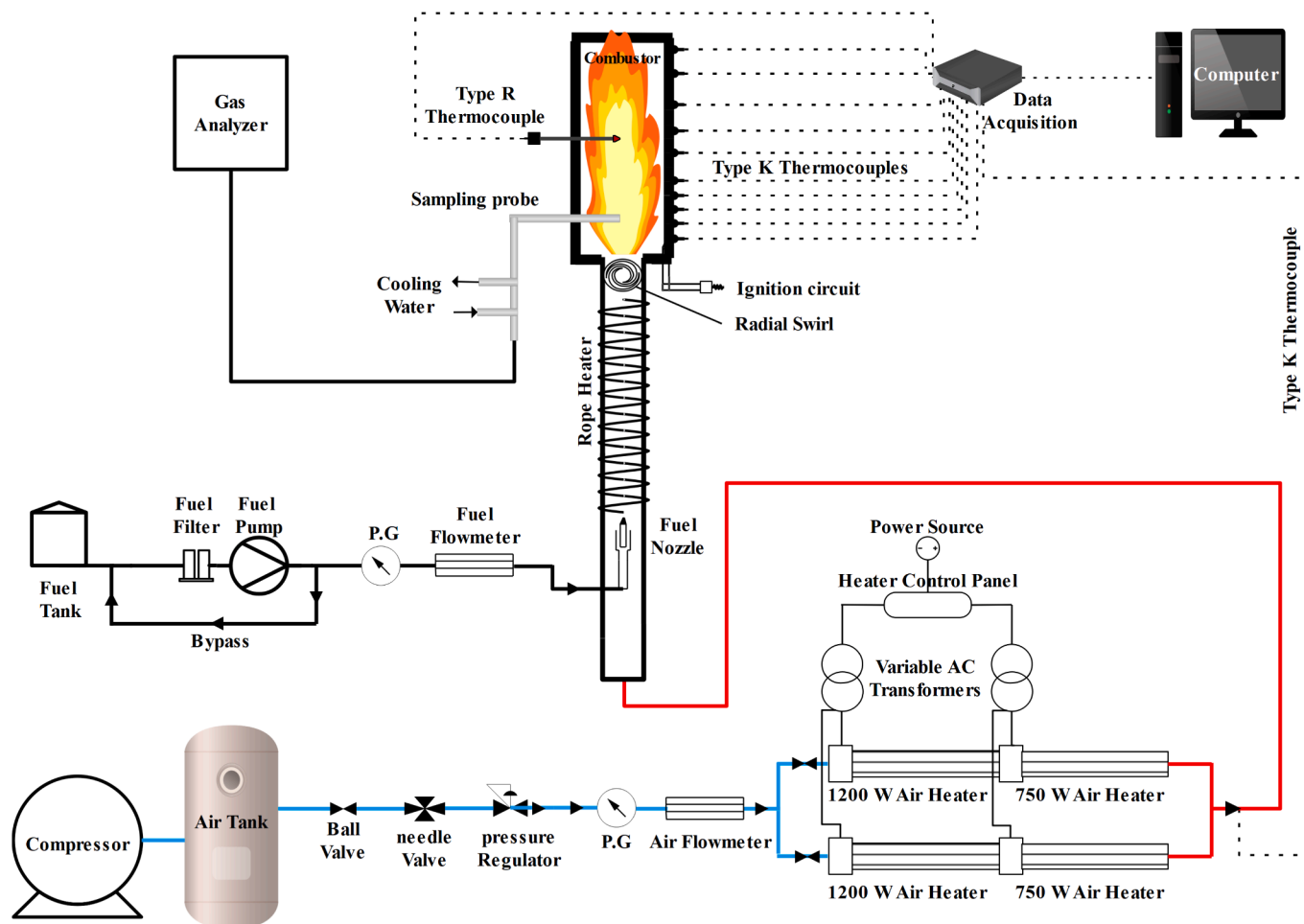
**Fig. 1.** Schematic diagram for test rig.

biodiesel, which is expected to reduce $NO_x$ production. Table 2 provides a summary of previous research on the effects of ether fuels on biodiesel. Zhan et al. [10] studied the effects of adding DEE and ethanol to biodiesel/diesel blends in a constant volume combustor, and they discovered that adding DEE to diesel/biodiesel blends speeds up the formation of small secondary droplets, which makes diesel biodiesel blends easier to atomize. Compared to diesel and biodiesel, DEE has decreased dynamic viscosity and surface tension, which causes the fuel droplets to split into more tiny droplets rapidly. Tran et al. [14] examined the effects of DEE as a pure biofuel and as a fuel additive on the production of pollutants and flame configuration in premixed combustion. They discovered that the number of hydrocarbons in flames containing DEE was much reduced. Using a common-rail fuel injection system in a constant-volume combustor, Guan et al. [16] investigated how adding DBE to soybean biodiesel affected spray properties on a macroscopic and microscopic scale. The findings demonstrated that DBE's decreased viscosity, density, and surface tension promote biodiesel atomization by minimizing SMD. Using a constant volume combustor and a mixing ratio of DBE between 0% and 40%, Gao et al. [16] also studied the impact of adding DBE to biodiesel on a laminar diffusion flame. The results of the experiment showed that the addition of DBE can reduce soot generation. Fu et al. [13] investigated the spraying properties of soybean biodiesel mixed with DBE at blending percentages of 15 and 30% in a constant-volume combustor. It was found that adding DBE made the spray tip penetration shorter and the spray cone angle wider.

According to previous findings, a lean premixed pre-vaporized (LPP) system can achieve low-temperature approaches and model gas turbine applications. Meanwhile, WCO biodiesel provides several benefits, such

as being accessible, renewable, cleaner energy sources, affordable to collect, and lower waste management expenses. But its viscosity and volatility are seen as its major drawbacks, which hinder its ability to be blended in large amounts with Jet A-1. In a single step, WCOME was prepared from WCO via a transesterification reaction employing sodium hydroxide as a catalyst and methanol. Then, DEE was added to biodiesel to improve its performance in continuous combustion systems, as suggested by Tran et al. [14] and Zhan et al. [10]'s research on the impact of DEE on biodiesel's spray properties and premixed flames. To the best of the authors' knowledge, there is no investigation found that studied the effects of adding DEE as an additive to a blend of Jet A-1 and WCO biodiesel. To fill this gap, the main contribution of this study is to enhance the utilization of WCO biodiesel in the LPP system using DEE as a fuel additive. With a volume blending ratio of 20%, DEE was added to Jet A-1/ WCOME. Finally, the combustion and emissions of the fuel blend were evaluated and compared to those of the biodiesel blend and Jet A-1.

## 2. Test rig and methodology

### 2.1. Test rig

To investigate the combustion characteristics of diethyether addition to the Jet A-1/WCOME blend, a combustor test rig was set up employing the LPP combustion technique and outfitted with the necessary measuring instruments, as shown in Fig. 1. The following is a brief description of the testing facility:

**Table 3**
Technical specifications of the devices used in the LPP system.

| Sn. | Equipment | Make/Model | Technical specifications |
|---|---|---|---|
| 1 | Oil pump | SUNTEC-AL | • Inlet Pressure 2 bar Return Pressure 2 bar Max Pressure 25 bar |
| 2 | Oil nozzle | Monarch series R | • Flow rate 0.5 USG/H Spray angle 45° |
| 3 | Air flowmeter | Dwyer DR4104 | • (1 ~ 16 scfm) flowrate range ±10% full-scale accuracy 121 °C temperature limit 13.8 bar pressure limit |
| 4 | Limited Pressure switch | Euro switch NO 4111122DI | • (0 ~ 10 bar) pressure range (0.1 bar) tolerance |
| 5 | Low temperature inline heater | Omega AHPF-122 | • 1200 W 240 VMaximum CFM is 15 |
| 6 | high temperature inline heater | Omega AHP-7562 | • 750 W 240 VMaximum CFM is 20 |
| 7 | Variable AC transformer | SEIDEN | • (0 ~ 240) Voltage range (0 ~ 8) Current range |

**Table 4**
Conditional parameters in the transesterification reaction.

| Alcohol | Oil to alcohol molar ratio | Catalyst type | Mixing method | Reaction temperature | Mixing duration |
|---|---|---|---|---|---|
| Methanol | 6:1 | 1% by weight of oil KOH | mechanical | 60℃ | 90 min |

i. Air delivery system: air is compressed by a screw compressor, model MSK-G22, into an accumulator tank. To obtain a steady air flow rate and avoid airflow fluctuations caused by tank pressure changes, a pressure regulating valve (model Euro switch NO 4111122DI) is fitted after the tank. A needle valve is installed after the PRV to fine-tune the air flow rate through the system. The inline air flowrate is evaluated with a Dwyer high-flow glass rotameter (Model DR4104) ranging from 1 to 16 CFM. A type T thermocouple coupled to a NI 9213 Data Acquisition Card (DAQ) and a pressure gauge are used to measure air temperature and pressure.

ii. Air heating system: The air is heated by four electric heaters in two separate paths. There are two sets of inline heaters per path, 1200 W (Omega AHPF-122) and 750 W (Omega AHP-7562). A limited pressure switch (Model Euro switch No 4111122DI) is used to ensure safe heating system operation. It is responsible for turning off heaters when there is no airflow. The air temperature is controlled by two variable AC-transformers (SEIDEN). A thermocouple (type K) measures the air temperature using the NI 9213 DAQ.

iii. Fuel delivery system: A 2-liter beaker is used to hold the fuel pumped to the oil nozzle by a fuel pump with a bypass line to reverse the extra fuel flow back. Two filters are located before and after the pump to remove any impurities before reaching the fuel pump and fuel nozzle, respectively, to avoid blockage of the fuel path. The fuel nozzle constantly atomizes fuel in the mixing tube at high pressure. With a 45-degree angle, the nozzle has a solid spray pattern and a rated flow rate of 0.5 Gal/h.

iv. Mixing tube: Through the mixing tube, the fuel is mixed with the hot air. To minimize heat loss to the surrounding, the mixing tube is insulated with 25 mm of ceramic thermal insulation. In addition, an additional heater is installed along the tube to keep the tube and hot air at the required temperatures.

v. Combustor: The confined steel tube has a bore of 150 mm and a length of 500 mm, whereas the swirl burner has a diameter of 16.1 mm. The burner has a radial swirler with eight 45°-angled straight vanes and a swirl number of 0.55. Temperature and species concentration are measured throughout the flame via five holes of 10-mm-diameter in the combustor's upper section and a 164-mm-long, 10-mm-wide groove in the lower section. Additionally, it has ten welded nuts and ten type K bolt thermocouples installed for continuously measuring the wall temperature.

Table 3 presents further technical details about the equipment used in the current study.

*2.2 Tested fuels*

Jet A-1 fuel, waste cooking oil biodiesel, and diethyl ether were used to investigate the combustion and emission characteristics of DEE addition to biodiesel. Misr Petroleum Company supplied the Jet A-1, and DEE was purchased locally, while the biodiesel was produced in the lab using waste cooking oil gathered from local homes and the transesterification method. In this work, the optimum parameters suggested by Attia and Hassaneen [20] were applied, and they can be found in Table 4. In addition, transesterification procedures are summarized in Fig. 2.

As shown in Fig. 3, Fig. 4 (conducted by Bruker), and Table 5, biodiesel was evaluated using thermogravimetric analysis (TGA), gas chromatography-mass spectrometry (GC–MS), and Fourier transform infrared spectroscopy. Fig. 3 shows that biodiesel starts to vaporize at 200 °C and completely evaporates at about 450 °C, particularly in comparison to 500 °C for raw oil. Thus, transesterification made oil more volatile. FTIR spectrometry can guarantee biodiesel production by identifying FAME groups [20]. Table 5 presents the results of the GC–MS analysis. This table shows the retention time and fragmentation pattern for the common abundant FAMEs. Fig. 4 also indicates that WCO has been converted to WCOME due to grouping indicative of methyl ester ($CO$-$O$-$CH_3$) at 1,452 $cm^{-1}$, ester stretch ($C = O$) at 1741 $cm^{-1}$, methyl (–$CH_3$) at 2,935 and 2,850 $cm^{-1}$, and hydroxyl (–$OH$) at 3,000–3,500 $cm^{-1}$.

As shown in Fig. 5, Jet A-1 and biodiesel were blended at a 20% blending ratio (W20), then 20% DEE and 20% biodiesel were mixed with 60% Jet A-1 (W20D20). The blending percentages of the test blends are presented in Table 6.

The chemical and physical properties of the prepared samples were determined and recorded in Table 7; these included viscosity at 40 ℃, density at 20 ℃, calorific value, flash point, and elemental analysis. The surface tension of mixtures was determined using Saxena et al.'s formula [21]. The heating value of fuel blends was determined using El-Maghraby's formula [22]. As can be seen in Table 7, Biodiesel is denser and more viscous than Jet A-1. Biodiesel has 8.7% less calorific value than diesel but 8.5% more than DEE. DEE has the lowest fuel-specific gravity, surface tension, and viscosity. The flash point of biodiesel is the highest. DEE has a much higher cetane number than biodiesel. Biodiesel contains 11.3% oxygen, compared to 21.6% in DEE. The blends' oxygen content, cetane rating, density, viscosity, and lower calorific value are all enhanced by adding more DEE.

To study the volatility of the tested fuels, a thermogravimetric analysis (also known as TGA) was carried out. The thermogravimetric analysis quantifies the magnitude and rate of a material's mass change in relation to temperature. A thermogravimetric analyzer (model Labsys
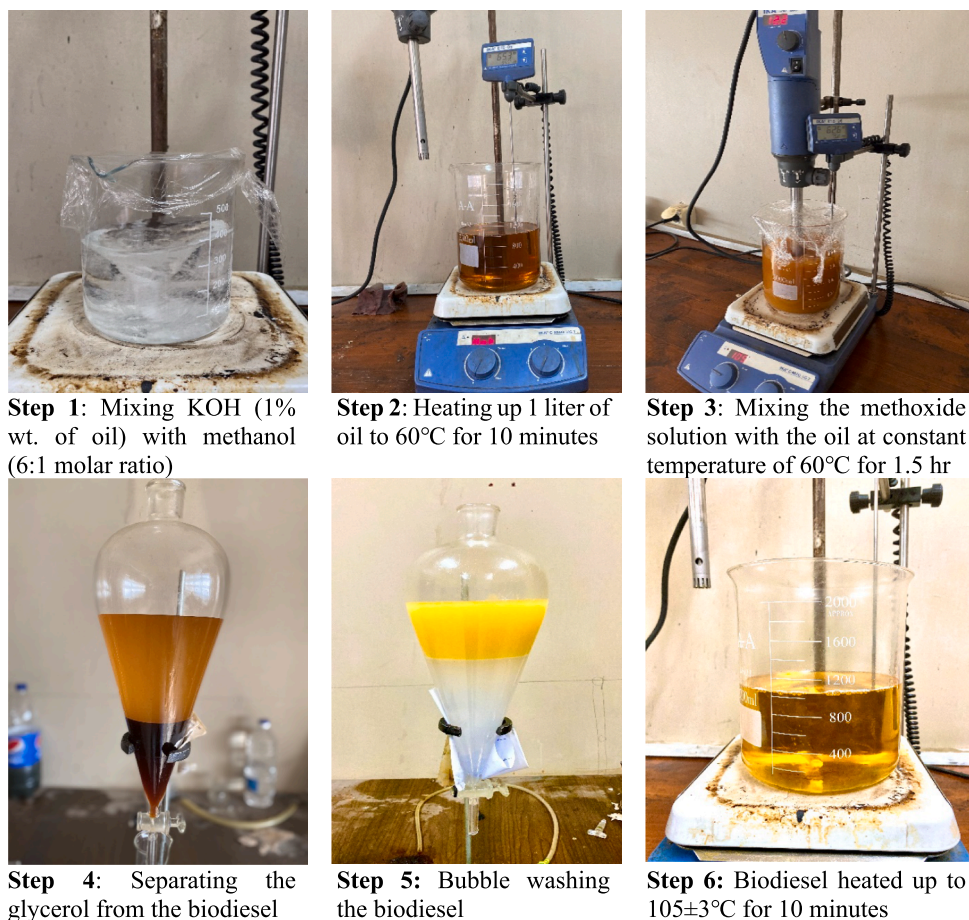
**Step 1**: Mixing KOH (1% wt. of oil) with methanol (6:1 molar ratio)

**Step 2**: Heating up 1 liter of oil to 60℃ for 10 minutes

**Step 3**: Mixing the methoxide solution with the oil at constant temperature of 60℃ for 1.5 hr

**Step 4**: Separating the glycerol from the biodiesel

**Step 5:** Bubble washing the biodiesel

**Step 6:** Biodiesel heated up to 105±3℃ for 10 minutes

**Fig. 2.** Photographic views of transesterification steps.
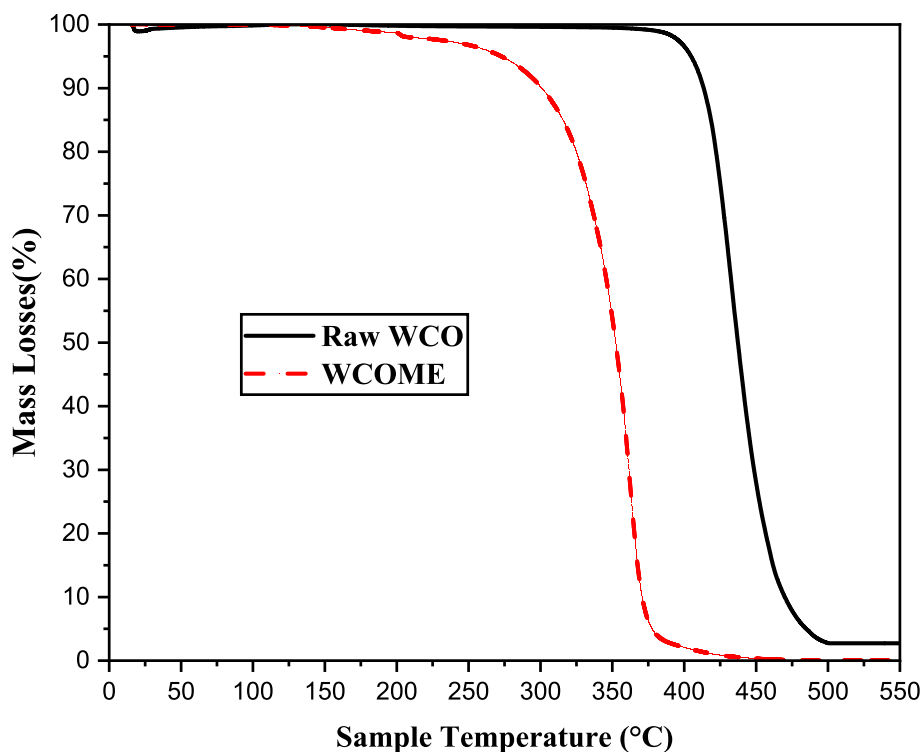


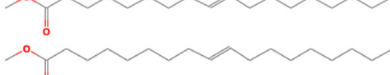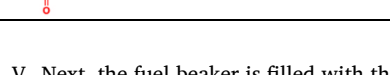**Fig. 3.** TGA results of raw WCO and WCOME.
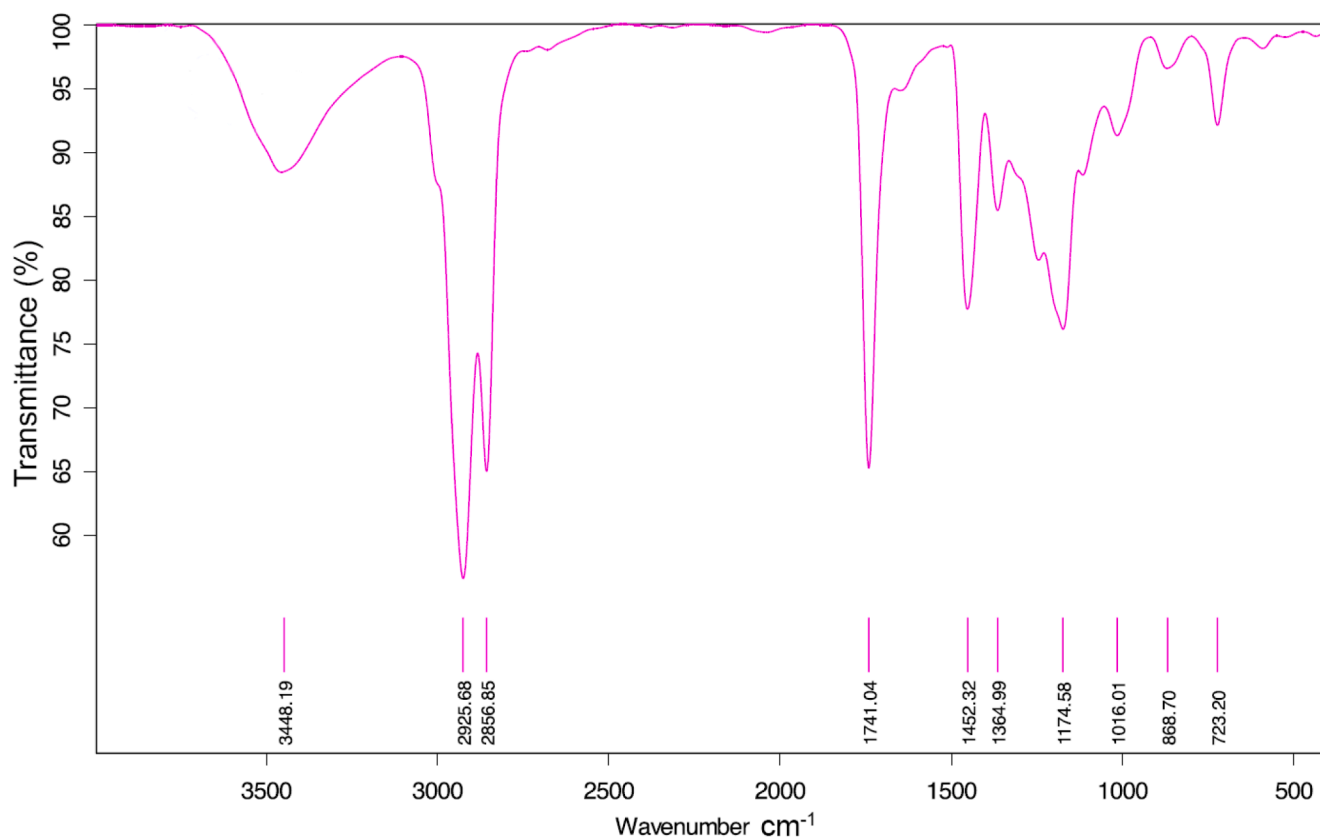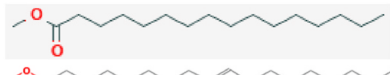
**Fig. 4.** FT-IR spectrum of WCOME.

**Table 5**
Composition and formula of fatty acid methyl esters derived from GC–MS analysis of WCO biodiesel.

| Common name | Retention time (min) | Structure | Formula |
|---|---|---|---|
| Methyl tetradecanoate | 9.75 | | $C_{15}H_{30}O_2$ |
| Hexadecanoic acid, methylester | 11.78 | | $C_{17}H_{34}O_2$ |
| 9-Octadecenoic acid, methyl | 13.679 | | $C_{19}H_{36}O$ |
| Methyl stearate | 13.881 | | $C_{19}H_{38}O_2$ |

Evo-Setaram) was used for this test. Fig. 6 presents TGA results for the sampled fuels. It is clear from the graph that Jet A-1 begins to evaporate at 120 °C and completely evaporates at 250 °C. Whereas the W20 blend fully evaporates at 340 °C. When DEE was added to W20D20, it started to evaporate at about 34 °C and finished at 340 °C. To avoid partial pre-vaporization, a preheated air temperature of 350 °C was selected to get a more complete vaporization.

### 2.3. Testing procedures and working conditions

The subsequent steps are followed to carry out the experiments:

  I. Air tank is drained of moisture.
 II. Adjusting the compressor to operate between 6 and 7 (bar).
III. The airflow rate is set to the desired amount.
 IV. Turning on the air heaters, setting the variable AC transformers to the desired voltage, and maintaining the air temperature at 350 ± 2℃.
  V. Next, the fuel beaker is filled with the test fuel.
 VI. Fuel pump operates to supply the system with fuel.
VII. Mixture is then ignited using ignition electrodes.
VIII. Regularly checking the flowrate of fuel and air to maintain a constant Φ of 0.85.
 IX. Taking the measurements of flame and emissions at the steady state at the sampling points with the help of the two-dimensional traverse mechanism.

Throughout the tests, the air temperature was kept at 350 ℃. This was the highest temperature that available air heaters could generate at this flow rate. Further, a steady flame was accomplished by modulating Φ as lean as possible, which was 0.85, and was held constant by varying the fuel flow rate while holding the air flow rate fixed. Experiment parameters are reported in Table 8.

**Fig. 5.** The two blends' samples.

**Table 6**
Volumetric mixing ratios of the tested fuels.

| Test fuels | Jet A-1 | Biodiesel | DEE |
|---|---|---|---|
| Jet A-1 | 100% | – | – |
| W20 | 80% | 20% | – |
| W20D20 | 60% | 20% | 20% |

## 2.4. Evaluation methodology

Temperatures (the flame temperature at various locations and combustion chamber wall temperature) beside local species concentrations were measured to describe the flame structure throughout the LPP combustor.

A ceramic insulated thermocouple - type R (platinum/platinum-13% rhodium) was used to measure the flame temperatures. The thermocouple has an accuracy of ± 1.5 °C, a wire diameter of 100 μm, and a bead diameter of 0.6 mm. The temperatures of the combustor wall were measured using 10 calibrated K-type thermocouples at different points along the combustion chamber wall. The temperature readings were recorded by the data acquisition card (Model NI USB-9213) at a rate of 100 samples per second. In addition, the measurement process was not started until the thermocouple temperature reached steady at each point. The average of the measured values was then calculated and

corrected against thermal radiation heat losses, then the mean of the actual temperatures was obtained using an approach followed by El-Zoheiry [23]. The flame temperatures were measured at 14 vertical levels, and each had 8 points in radial direction based on the grid in Fig. 7(a).

A stainless steel sampling probe cooled by water was used to collect the hot product gases from 8 levels, each including 8 points in radial directions, as described in Fig. 7(b). These sampling levels were selected to be only 8 levels as they were enough to explain the flame's emission characteristics. A gas analyzer (Model ECOM-J2KN Pro) was coupled to the sampling probe and supported by a filtration system and condensate trap to ensure that the gas analyzer instrument operated safely, hence sucking only dry samples. Species concentrations were recorded by the gas analyzer at a rate of 30 samples per minute, and the average values were obtained from these measured values. Table 9 shows the specifications of the gas analyzer. Since the sampling probe has a diameter of 8 mm and is water-cooled, the impact caused by thermal radiation on the
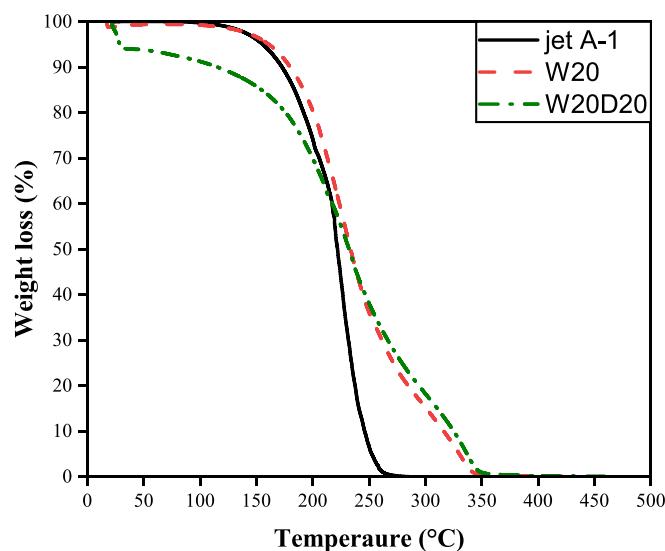


**Fig. 6.** Tested samples' TGA.

**Table 8**
Experimental operating conditions.

| # | Fuel | $\dot{m}_f$ (kg/hr) | $\dot{m}_a$ (kg/hr) | $T_a$ (°C) | Φ |
|---|---|---|---|---|---|
| 1 | Jet A-1 | 1.23 | 21.04 | 350 | 0.85 |
| 2 | W20 | 1.26 | | | |
| 3 | W20D20 | 1.32 | | | |

**Table 7**
Chemical and physical characteristics of the tested fuels.

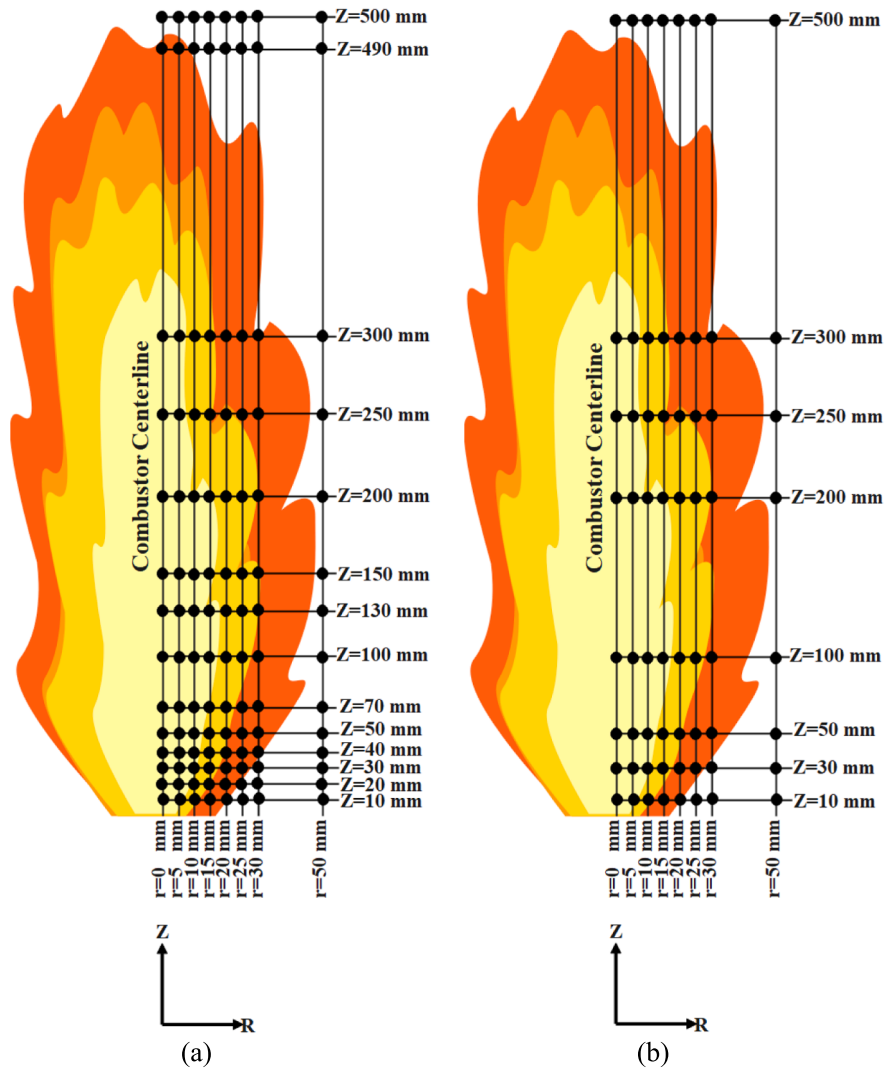| Specification | Unit | Jet A-1 | WCOME | DEE | W20 | W20D20 |
|---|---|---|---|---|---|---|
| **Viscosity at 40 °C** | [cSt] | 1.080 | 3.140 | 0.230 | 1.2 | 1.063 |
| **Density at 20 °C** | [kg/m³] | 797 | 877 | 715 | 813.7 | 802.5 |
| **Surface tension** | [N/m] | 0.0265 | 0.0341 | 0.0148 | 0.0280 | 0.0254 |
| **Flash Point** | [°C] | 39 | 130 | −40 | – | – |
| **Cetane number** | – | | 46 ~ 48 | 51 | 120 | – | – |
| **Lower heating value** | [MJ/kg] | 43.46 | 39.98 | 36.84 | 42.32 | 41.59 |
| **Molecular mass** | [kg/kmol] | 148.0 | 290.9 | 74.12 | 176.6 | 161.8 |
| **Element analysis** | [%] by mass | | | | | |
| Carbon | | 86.51 | 77.22 | 64.9 | 85.18 | 80.83 |
| Hydrogen | | 13.48 | 11.46 | 13.5 | 13.29 | 13.30 |
| Sulfur | | Nil | Nil | Nil | Nil | Nil |
| Oxygen | | Nil | 11.3 | 21.6 | 1.516 | 5.861 |
| Nitrogen | | Nil | Nil | Nil | Nil | Nil |
| **A/F$_{stio}$** | | 14.53 | 13.18 | 11.14 | 14.52 | 13.56 |
| **H/C** | | 1.87 | 1.89 | 2.49 | 1.88 | 1.97 |

**Fig. 7.** Sampling locations of (a) temperature and (b) species.

**Table 9**
Technical data of the gas analyzer.

| Sensors | Range | Resolution | Maximum uncertainty (%) | Theory |
|---------|-------|------------|-------------------------|--------|
| $CO_2$ | 0 to 20 % by volume | 0.1% by volume | 0.5 | IR |
| CO | 0 to 6.3% by volume | 0.01% by volume | 0.16 | IR |
| $O_2$ | 21% by volume | 0.1 % by volume | 0.48 | Electrochemical |
| $NO_2$ | 0 to 1000 (ppm) | 1 (ppm) | 0.1 | Electrochemical |
| NO | 0 to 5000 (ppm) | 1 (ppm) | 0.02 | Electrochemical |

precision of the temperature readings would be considerable. For this reason, it is often recommended to take separate temperature and species concentration readings.

A total uncertainty of the experiment was carried out using the following equation deduced by Kline [59]:

$$W_R = \sqrt{\left(\frac{\partial R}{\partial x_1}W_{x_1}\right)^2 + \left(\frac{\partial R}{\partial x_2}W_{x_2}\right)^2 + \cdots + \left(\frac{\partial R}{\partial x_n}W_{x_n}\right)^2} \quad (1)$$

Where $W_R$ is the uncertainty of the experimental result, and R is the given function of the observed values ($x_1, x_2$, and $x_n$). In this work, an uncertainty analysis is conducted on temperature and species concentration measurements. The maximum temperature uncertainty was 0.735%, while the maximum species concentration uncertainties were listed in Table 9.

## 3. Results and discussion

### 3.1. Combustion characteristics

Flame temperature is a vital combustion feature that helps study other combustion properties and pollutants. A contour plot of the FTD of the tested fuels is presented in Fig. 8. The flame shape of the W20 blend is shown in the figure to be wider than that of Jet A-1 and to have higher flame temperatures at lower levels. While the flame shape of the W20D20 blend is shown to be similar to that of Jet A-1, but with relatively lower temperatures. The highest flame temperature was recorded with Jet A-1, followed by W20 and W20D20 blends.

To provide a more in-depth description of the combustion, the flame temperature is plotted against the axial distance of the combustor at various radial positions in Fig. 9. As shown, the flame can be categorized into three zones [24]:
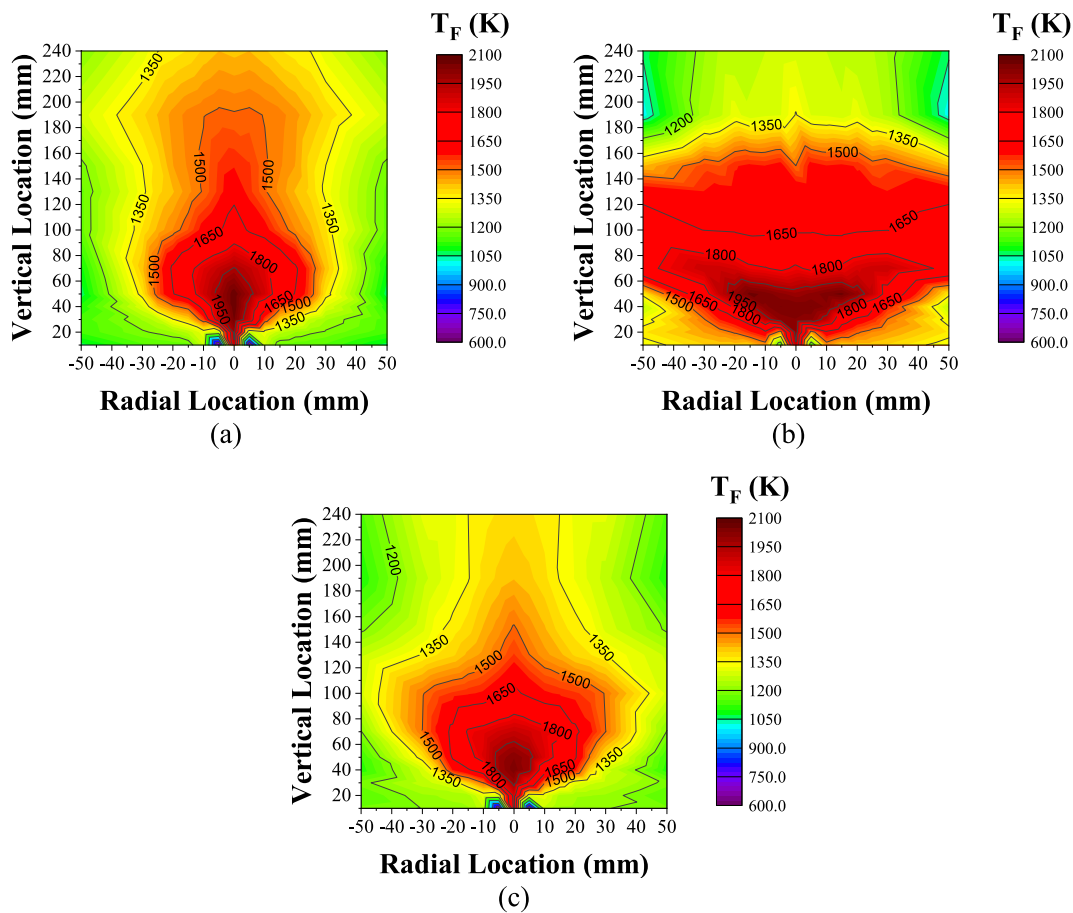
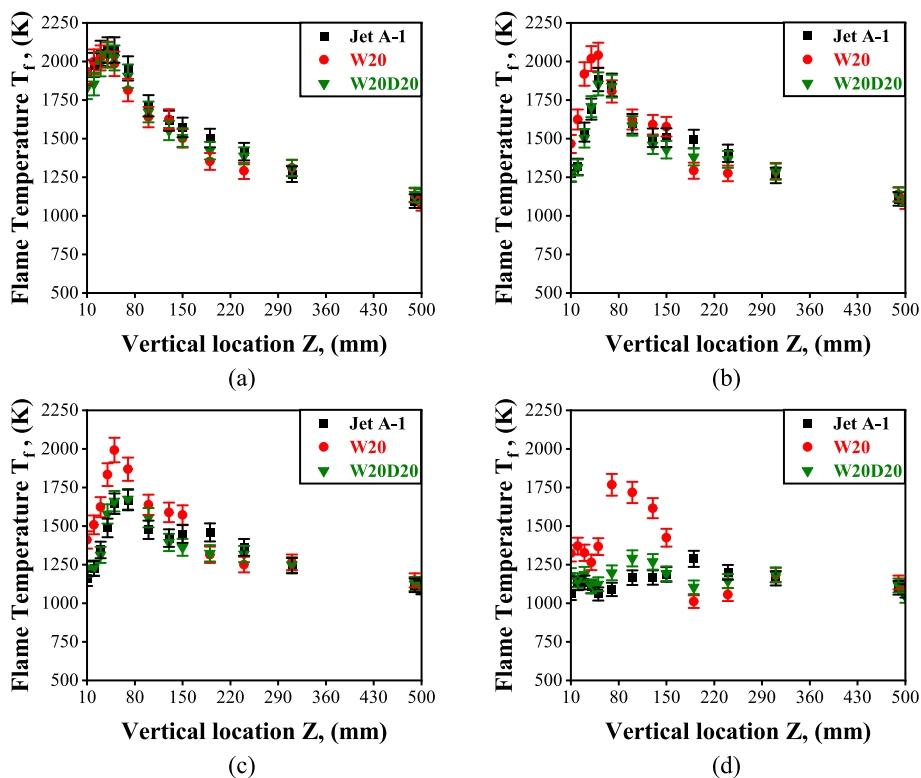**Fig. 8.** Contours plot of FTD of (a) Jet A-1, (b) W20, and (c) W20D20.



**Fig. 9.** Axial FTD of the tested fuels at (a) r = 0, (b) r = 10, (c) r = 20, and (d) r = 50 mm.
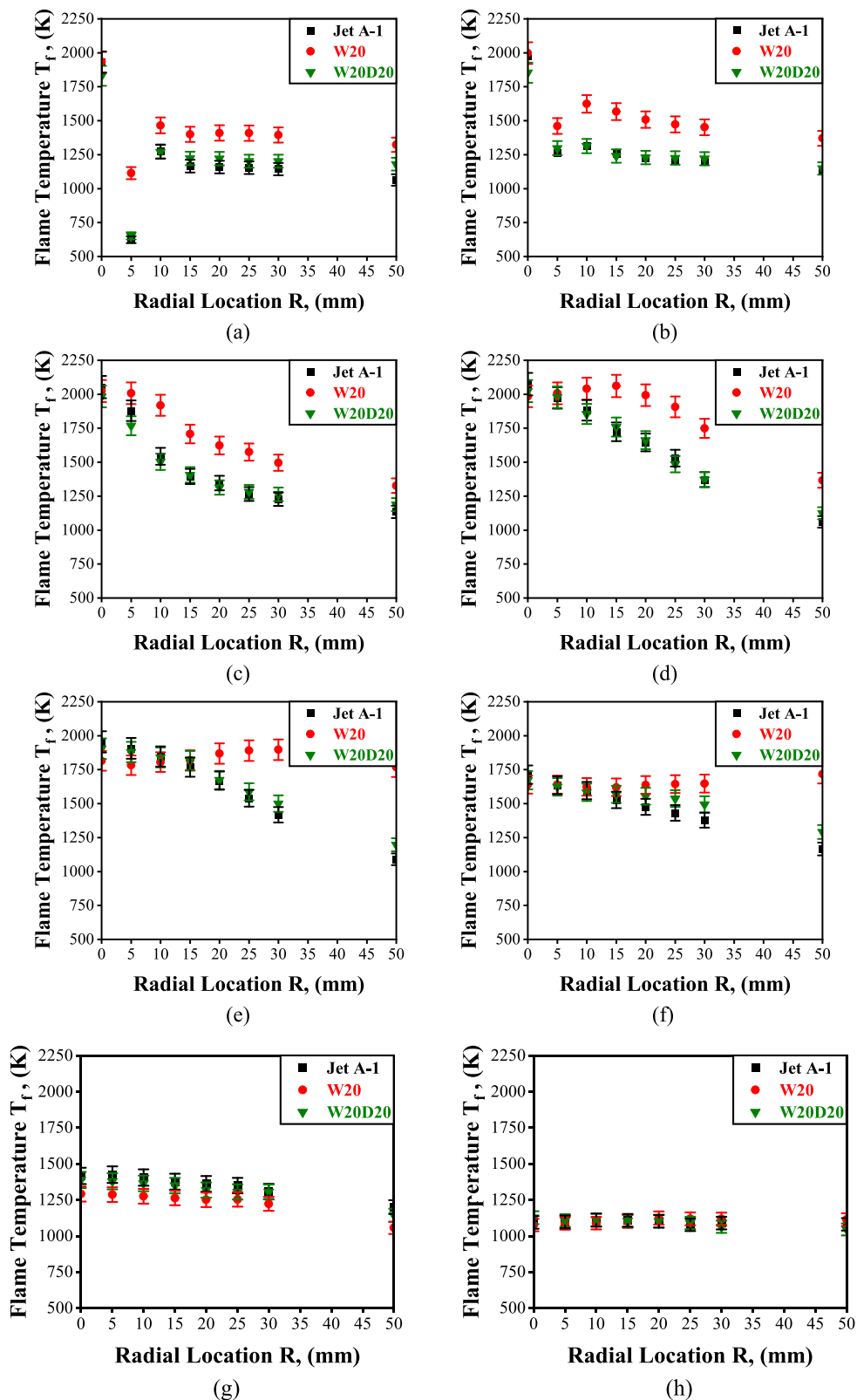
**Fig. 10.** Radial FTD of the tested fuels at Z= (a) 10, (b) 20, (c) 30, (d) 50, (e) 70, (f) 100, (g) 250, and (h) 500 mm above the burner.

1. Flame initiation zone that initiates the oxidation process between the pre-mixed reactants. Due to non-thermal equilibrium reactions in this zone, free radicals are concentrated [25]. This zone is above the burner and is close to 20 mm long. The oxidation rate keeps rising in this zone, reaching a maximum in the following area and with steep temperature gradients. The addition of DEE reduces the temperature in this zone.

2. In the flame recirculation zone, the maximum flame temperatures are attained at about 40 mm above the burner; the flame temperature
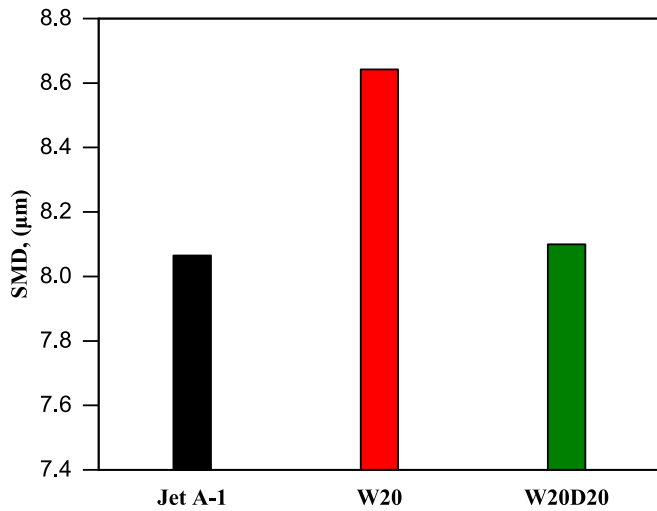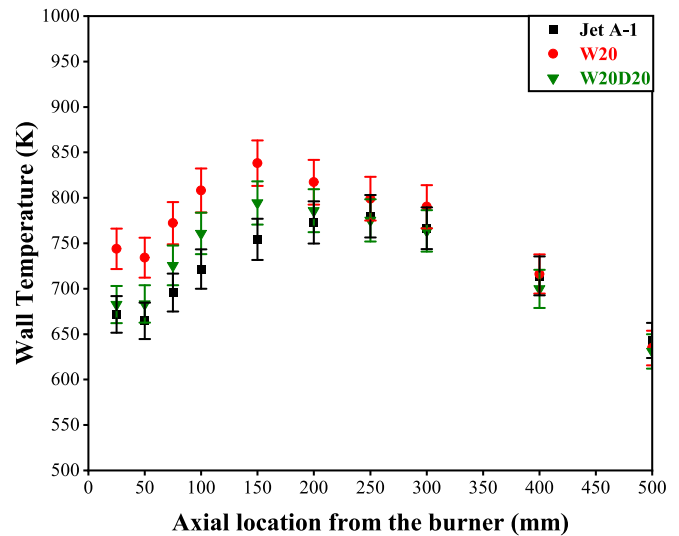
**Fig. 11.** SMD of the tested fuels.



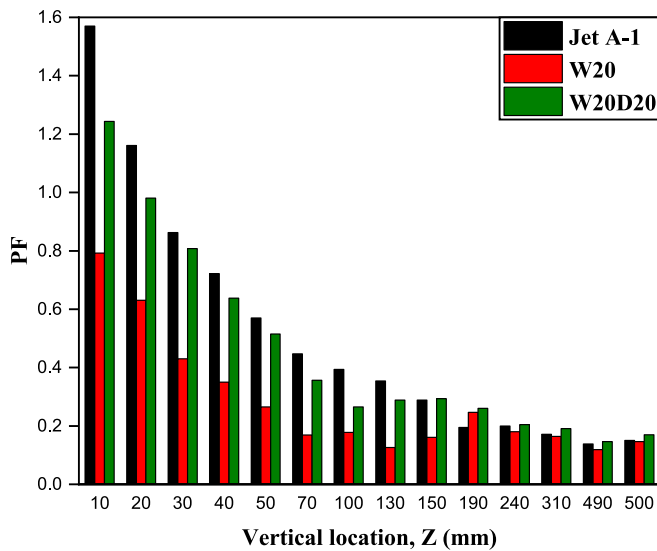**Fig. 13.** Wall temperature profile of the tested fuels.



**Fig. 12.** Pattern factor for tested fuels along the combustor.

decreases within the third zone. Adding DEE to the Jet A-1/biodiesel blend lowers the maximum flame temperature.

3. Post-flame zone where the flame temperature drops due to the wall's convection heat losses. This zone is 240 mm above the burner. After that level, the flame temperature begins to decline due to convection heat losses to the wall, and the flame gradually vanishes.

The FTD in the radial direction throughout the combustor is also plotted in Fig. 10. The temperatures are low at lower levels of all radial positions, where the initiation reactions are still occurring and quickly increasing. Furthermore, Jet A-1 had a peak flame temperature of 2,074 k, while the peak temperatures for W20 and W20D20 blends were 2,061 K and 2,041 K, respectively, these temperatures were all achieved at Z = 40 mm.

Despite biodiesel having a lower heating value compared to Jet A-1, W20 consistently produced a hotter flame, measuring up to 70 mm above the burner. It then began to decrease steadily. One possible reason is that the biodiesel was not atomized well enough, resulting in fuel droplets that do not have the necessary energy and time for complete evaporation before reaching the flame zone. As a result, partial diffusion combustion occurs at the surface droplets with stoichiometric conditions

when these droplets combine with the air in the combustion chamber, and the flame temperature becomes higher than it would be under the lean combustion of Jet A-1. These droplets produced by inadequate atomization are significantly heavier, so the incoming air's inertia cannot carry them vertically throughout the combustion chamber while the swirler generates angular momentum. As a result, they create hot spots in the combustor wall by escaping radially toward the wall, where they can combust away from the burner's centerline. At higher levels, the FTD approaches the temperature of Jet A-1 as the biodiesel droplets gradually evaporate and the heterogeneous mixture dissipates. In addition, the higher adiabatic flame temperature of the W20 blend may be related to the higher number of double bonds present in biodiesel [26,27].

The addition of 20% DEE decreased the flame temperature of the W20D20 blend, but it remained higher than Jet A-1 at most levels. One reason for this is that DEE has a lower calorific value and a higher latent heat of vaporization, and this makes the fuel droplets absorb more heat from the surrounding air to evaporate and ignite, reducing the heat released from the combustion [28]. Hence, the flame temperature decreases. As a result, the temperature profile of the W20D20 blend is much closer to that of the Jet A-1. Another factor contributing to the decrease in temperature of the W20D20 combination is greater atomization, a smaller SMD, an increased evaporation rate, and better fuel and air mixing, which ultimately results in a homogeneous mixture since adding DEE has reduced the fuel's viscosity and surface tension. This drop in viscosity and surface tension enhances the atomization degree, which enhances the rate of fuel evaporation and the homogeneity of fuel and air mixing. Then, the fuel combusts again in the combustor using a premixed combustion mode, unlike W20's partially diffusion combustion mode of unevaporated fuel droplets.

$$ SMD = 2.25\sigma^{0.25}\mu_l^{0.25}\rho_a^{-0.25}\Delta P_l^{-0.5}m^{0.25} \tag{2} $$

Sauter Mean Diameter (SMD), which is the most effective parameter to reflect the quality of atomization, could be computed for test fuels using the following equation derived by Lefebvre and Ballal [29]:

Fig. 11 shows the SMD of the tested fuels. It was found that the SMD for the W20 blend was the highest (8.64 µm), while the SMD for the W20D20 mixture and Jet A-1 was the lowest (8.06 µm). It meant that the SMD increased by 7.2% when 20% WCO biodiesel was added to Jet A-1 and decreased by 6.7% when 20% DEE was added to the W20 blend. Since DEE has a lower surface tension than WCOME and Jet A-1 (0.014868 N/m, 0.03412 N/m, and 0.0265 N/m, respectively), the DEE blend atomizes more efficiently. Additionally, DEE is less viscous than
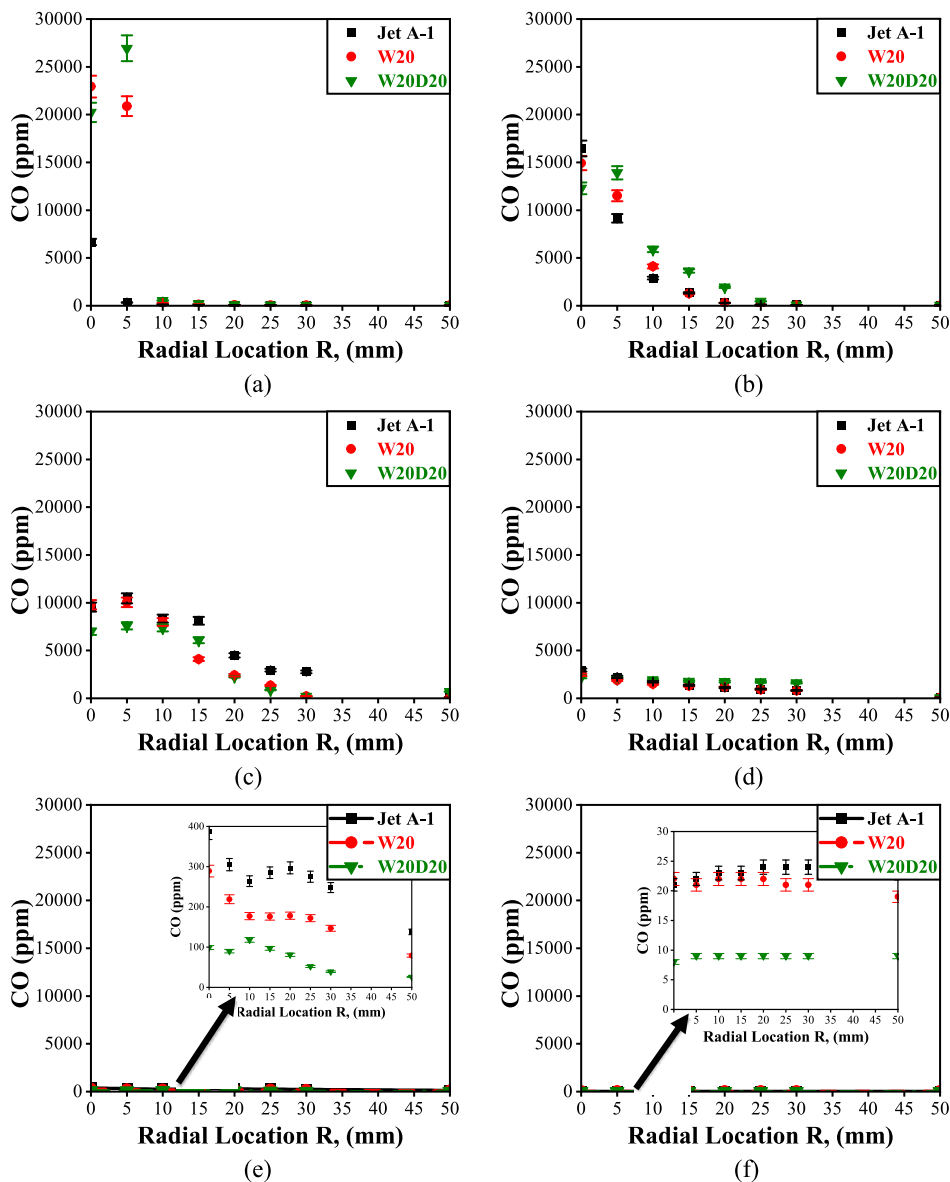
**Fig. 14.** Distribution of CO radially along the combustion chamber at Z= (a) 10, (b) 30, (c) 50, (d) 100, (e) 200, and (h) 500 mm above the burner.

WCOME and Jet A-1, as previously shown in Table 7.

The pattern factor (PF), which represents how uniform the temperature is within the combustor, is one of the essential parameters that must be taken into consideration in gas turbine combustion [29]. The test fuels were PF-calculated at different levels through the combustor. The better the combustor thermal homogeneity, the lower the PF [29]. This formula can be used to determine the PF:

$$PF = \frac{T_{max} - T_{min}}{T_{mean} - T_{in}} \qquad (3)$$

Fig. 12 demonstrates that the pattern factor trend begins with a high value and steadily drops throughout the combustion chamber for all evaluated fuels. In addition, the W20 blend has the lowest pattern factor of all the evaluated fuels. This is due to the combustion of WCOME droplets in the lower zone of the combustion chamber. Fig. 12 further shows an increasing impact of DEE on the pattern factor. Because DEE helps improve fuel atomization and reduces combustion droplets besides having a lower calorific value, which causes the flame temperature to drop, particularly close to the combustor wall, increasing the pattern factor.

### 3.2. Wall temperature profile

Testing different fuel blends affect the wall temperature distribution even while the equivalence ratio is fixed at 0.85. In all test fuels, the wall temperature increases and reaches its peak, creating hot spots at the wall due to the extreme heat intensity at this point. Then, it begins to drop gradually up to the combustion chamber outlet, as shown in Fig. 13. It was also observed that the addition of 20% WCO biodiesel to Jet A-1 raised the wall temperature and caused a deviation from the Jet A-1 profile, whereas adding 20% DEE to the Jet A-1/biodiesel blend reduced the wall temperature and made it closer to Jet A-1. Also, the maximum wall temperatures achieved were by W20 at 838.1 K, followed by W20D20 at 794.4 K, and Jet A-1 at 779.7 K. This is because the biodiesel has poor atomization, which causes larger droplet sizes that do not have enough time or energy for evaporation prior to approaching the flame zone. So, combustion inside the combustor is partially diffusion at stoichiometric condition at the surface, and the flame achieves a higher peak temperature compared to lean combustion of Jet A-1. This higher flame temperature of W20 raises the wall temperature. While the decreased wall temperature of W20D20 blend can be explained that
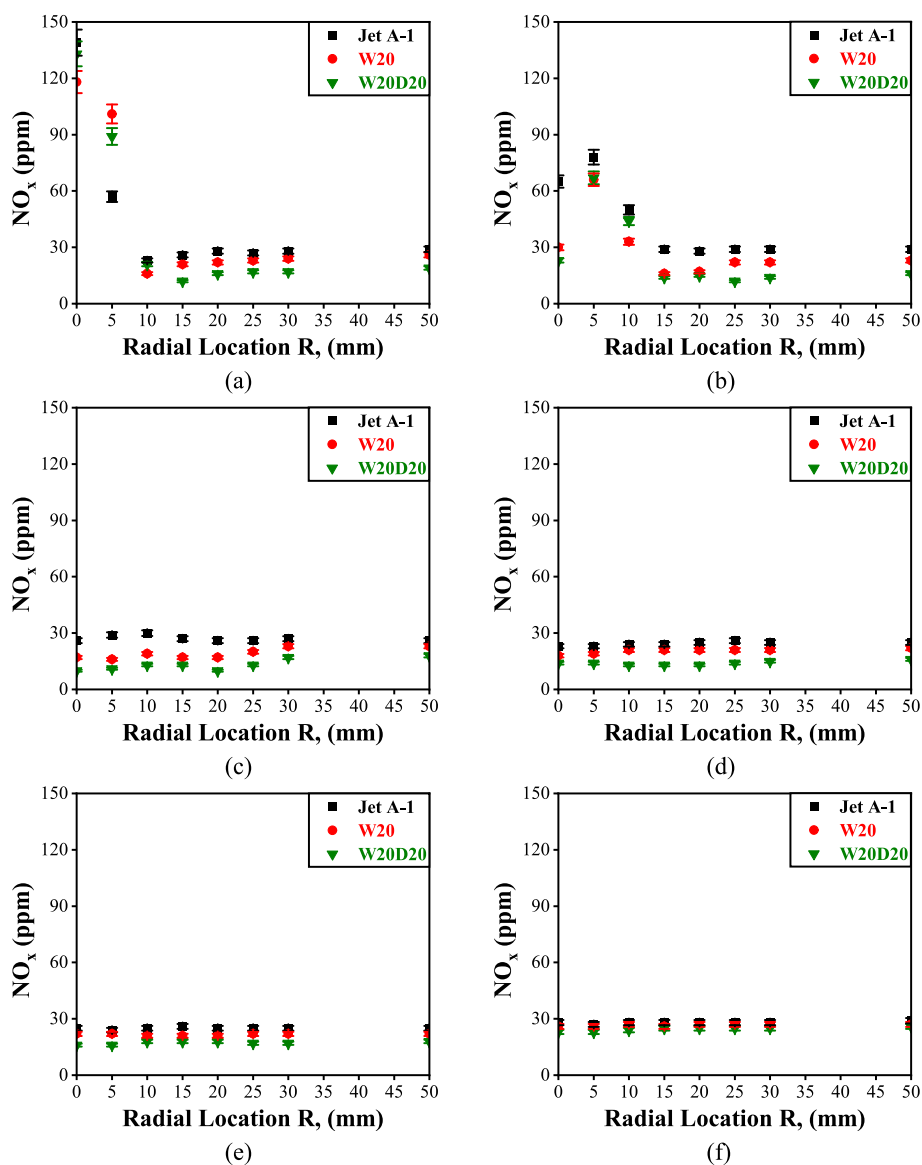
**Fig. 15.** Distribution of $NO_x$ radially along the combustion chamber at Z= (a) 10, (b) 30, (c) 50, (d) 100, (e) 200, and (f) 500 mm above the burner.

adding DEE enhances the fuel atomization due to its lower surface tension and viscosity. This helps the fuel evaporate more completely, creating more homogeneous mixtures. So, a premixed combustion approach is used to combust the fuel in the combustor, unlike W20's partially diffusion combustion of non-fully evaporated fuel droplets, and the flame temperature decreases, which reduces the wall temperature. Also, DEE has a lower heating value, which causes the flame temperature to decrease, so the wall temperature declines. The wall temperature profile also indicates the size of the flame formed. It is also observed that W20 is the widest flame, followed by W20D20 and Jet A-1, and the contour plot in Fig. 8 also confirms this.

### 3.3. Emission characteristics

Various parameters, involving fuel type, equivalence ratio, flow field, inlet, preheat air, flame temperatures, and the degree of atomization process, mainly affect the emission characteristics of the swirling LPP combustion [30]. Our study examines the effects of DEE as a fuel additive to the Jet A-1/biodiesel blend on CO, $NO_x$, and UHC while maintaining the other conditions listed in Table 8.

CO is formed during the oxidation of carbon to $CO_2$. Also, CO can be created when $CO_2$ dissociates in zones where the flame temperature is higher than 1800 K. Fig. 14 shows CO concertation (ppm @ 15% $O_2$ level) radially within the flame. At lower levels, there is a greater amount of CO due to the availability of much oxygen content, free radicals, and elevated temperatures that boost $CO_2$ dissociation. In contrast, it decreases progressively throughout the combustor at higher levels due to mixture homogeneity, free radical consumption, and lower flame temperatures. Also, CO levels drop near the wall of the combustor, where the flame temperature decreases.

Additionally, it is observed that the swirling recirculation zone causes the CO distribution to fluctuate arbitrarily up to 100 mm above the burner. This altitude has been recognized by Johnson et al. [31]. Beyond Z = 100 mm, W20D20 and W20 blends had 68% and 7% less CO concentration at the combustor outlet, respectively, compared to Jet A-1. This may be because DEE has a greater cetane number, more oxygen molecules, and lower viscosity and density than biodiesel blend, which, together with adequate fuel and air mixing and improved spray atomization, tend to result in lower CO emissions [1,9].

The Zeldovich mechanism produces thermal $NO_x$ at elevated temperatures of about 1,850 K, and the prompt $NO_x$ mechanism is the primary $NO_x$ generation mechanism in LPP combustion [29]. Thermal $NO_x$
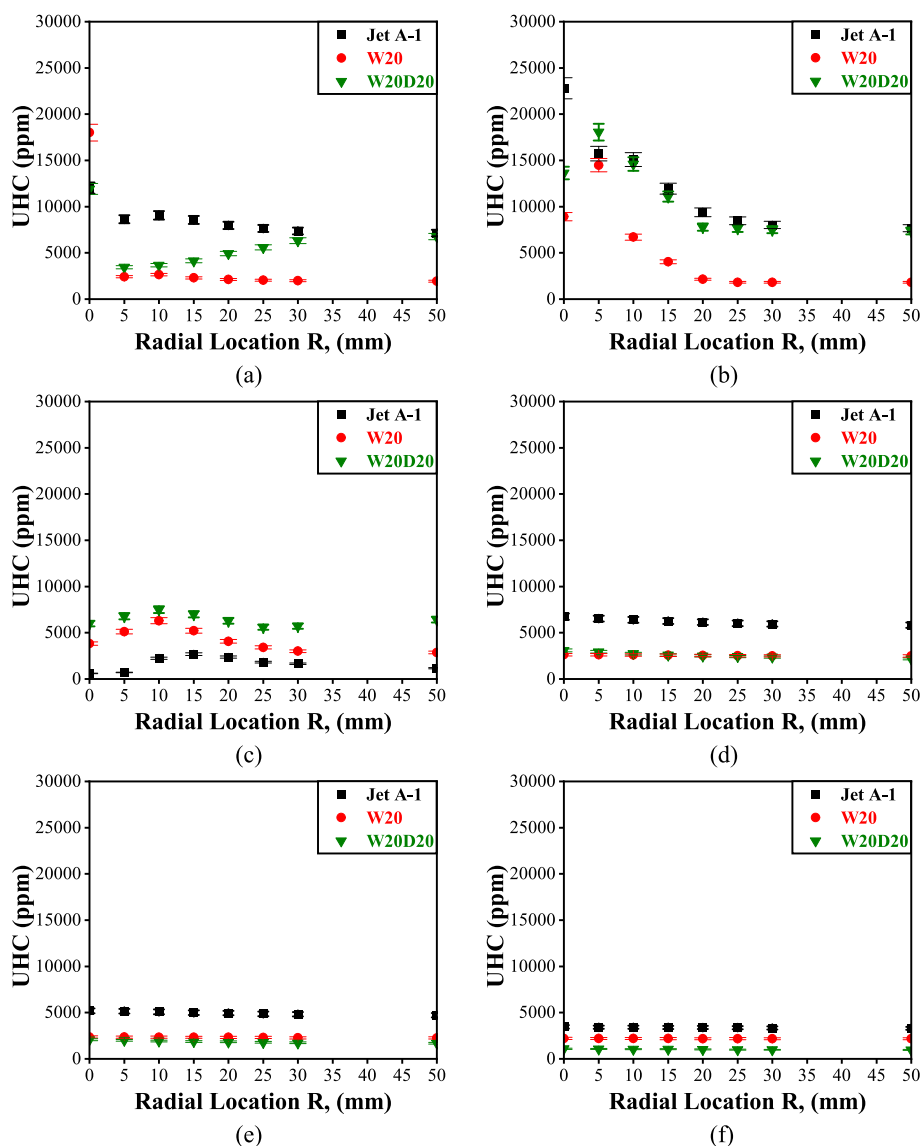
**Fig. 16.** Distribution of UHC radially along the combustion chamber at Z= (a) 10, (b) 30, (c) 50, (d) 100, (e) 200, and (h) 500 mm above the burner.

is affected by various parameters, such as the adiabatic and local flame temperatures, turbulence intensity, oxygen availability, residence time, the quality of spray, and the equivalence ratio within the flame [29 32]. Fig. 15 demonstrates how $NO_x$ (in ppm @ 15% $O_2$ level) initially rises at lower levels before steadily falling with vertical distance and achieving a minimal value at the combustor outlet. Furthermore, the W20 blend had a lower $NO_x$ concentration than that Jet despite its higher initial temperature, while the W20D20 mixture had the lowest $NO_x$ concentration overall, dropping by 12.5% relative to Jet A-1. The larger cetane number of DEE can be credited with the primary reduction in $NO_x$ concentration by shortening the ignition delay and premix formation time, lowering temperature peaks [32]. DEE's high latent heat of vaporization also aids in lowering combustion temperatures, resulting in reduced thermal $NO_x$ emissions [32]. Also, as shown in Table 7, DEE has 25% less carbon than Jet A-1, which decreases the propensity for prompt $NO_x$ generation, which is produced when hydrocarbon fragmentation combines with nitrogen to create nitrogen compounds, while the W20 blend has only a 10.7% less carbon content than Jet A-1 [33].

The term "unburned hydrocarbons" (UHC) includes the unburned fuel which escapes from the combustion chamber as tiny droplets or in the vapor phase and the lower molecular weight byproducts of the fuel's thermal degradation [29]. Some parameters dominate UHC, including

the characteristics of the fuel, poor atomization, improper burning rate, and the degree of homogeneity of the mixture [29]. In Fig. 16, UHC varies randomly due to the recirculation zone's influence. Additionally, it was found that the W20D20 blend reduced UHC emissions by approximately 69.6%, whereas the W20 blend only reduced UHC emissions by 35.3% as compared to Jet A-1. This may be explained by DEE's increased oxygen content, which is required to initiate the fuel's unsaturated hydrocarbons for more complete combustion [34].

## 4. Conclusions

The physical properties of DEE are impressive for combustion, which makes it a better jet fuel than conventional jet fuels. In this study, 20% DEE was mixed with biodiesel and Jet A-1 to explore the impact of DEE addition on combustion properties in a swirl-stabilized LPP combustor and compare it to Jet A-1. Jet A-1, W20, and W20D20 blends were all burned in an LPP combustor with the same air temperature of 350℃ and Φ (0.85). Combustor flame temperatures, and species concentration profiles are studied in detail. The following were the results of the analysis of the data:

1. Biodiesel's physicochemical properties, such as viscosity, surface tension, and SMD, were improved by 11.4%, 9.3%, and 6.7%, respectively, for the W20D20 blend relative to the W20 blend.

2. Compared to Jet A-1, DEE blends had similar FTD, but the W20 blend had a slightly different pattern. The highest flame temperature was recorded with Jet A-1 (2,074 K), while the lowest was with the W20 mixture (2,061 K). The W20 blend had a lower pattern factor, indicating more uniform temperatures throughout the combustor.

3. At the combustor outlet, the W20D20 blend had 61.4% less CO than Jet A-1, with an average value of 9 ppm compared with 23 ppm for Jet A-1 and 12.5% less $NO_x$ than Jet A-1, with an average value of 25 ppm compared with 28 ppm for Jet A-1.

4. UHC levels decreased by 69.6% compared to Jet A-1 with 20% DEE at the combustor outlet, with average values of 1,029 and 3,390 ppm, respectively.

The current findings strongly recommend adding DEE to biodiesel blends as an oxygenated fuel additive for improved and cleaner combustion.

## CRediT authorship contribution statement

**Radwan M. EL-Zohairy:** Conceptualization, Formal analysis, Investigation, Methodology, Supervision, Writing – original draft, Writing – review & editing, Data curation. **Ahmed S. Attia:** Conceptualization, Formal analysis, Investigation, Methodology, Supervision, Writing – original draft, Writing – review & editing, Data curation. **A.S. Huzayyin:** Conceptualization, Data curation, Supervision, Writing – review & editing. **Ahmed I. EL-Seesy:** Conceptualization, Formal analysis, Investigation, Methodology, Supervision, Writing – original draft, Writing – review & editing, Data curation.

## Declaration of Competing Interest

The authors declare that they have no known competing financial interests or personal relationships that could have appeared to influence the work reported in this paper.

## Data availability

Data will be made available on request.

## References

[1] Sivalakshmi S, Balusamy T. Effect of biodiesel and its blends with diethyl ether on the combustion, performance and emissions from a diesel engine. Fuel 2013;106: 106–10. https://doi.org/10.1016/j.fuel.2012.12.033.

[2] Kumar M, Karmakar S. Combustion characteristics of butanol, butyl butyrate, and Jet A-1 in a swirl-stabilized combustor. Fuel 2020;281:118743. https://doi.org/10.1016/j.fuel.2020.118743.

[3] Lin L, Cunshan Z, Vittayapadung S, Xiangqian S, Mingdong D. Opportunities and challenges for biodiesel fuel. Appl Energy 2011;88:1020–31. https://doi.org/10.1016/j.apenergy.2010.09.029.

[4] Habib Z, Parthasarathy R, Gollahalli S. Performance and emission characteristics of biofuel in a small-scale gas turbine engine. Appl Energy 2010;87:1701–9. https://doi.org/10.1016/j.apenergy.2009.10.024.

[5] Mohamed M, Sherif N, Aboelazayem O, Elazab HA, Gadalla M, Saha B. Waste Cooking Oil Management in Egypt: Production of Biodiesel-Development of Rapid Test Method. J Phys Conf Ser 2022;2305(1). https://doi.org/10.1088/1742-6596/2305/1/012035.

[6] Szalay D, Fujiwara H, Palocz-Andresen M. Using biodiesel fuel for gas turbine combustors. Landbauforsch Volkenrode 2015;65:65–76. https://doi.org/10.3220/LBF1443169529000.

[7] Gupta KK, Rehman A, Sarviya RM. Bio-fuels for the gas turbine: A review. Renew Sustain Energy Rev 2010;14:2946–55. https://doi.org/10.1016/j.rser.2010.07.025.

[8] Li H, Altaher M, Andrews GE. Evaluation of combustion and emissions using biodiesel and blends with kerosene in a low nox gas turbine combustor. Proc ASME Turbo Expo 2010;1:545–53. https://doi.org/10.1115/GT2010-22182.

[9] Qi DH, Chen H, Geng LM, Bian YZ. Effect of diethyl ether and ethanol additives on the combustion and emission characteristics of biodiesel-diesel blended fuel

[10] Zhan C, Feng Z, Ma W, Zhang M, Tang C, Huang Z. Experimental investigation on effect of ethanol and di-ethyl ether addition on the spray characteristics of diesel/biodiesel blends under high injection pressure. Fuel 2018;218:1–11. https://doi.org/10.1016/j.fuel.2017.12.038.

[11] Agarwal AK, Chaudhury VH. Spray characteristics of biodiesel/blends in a high pressure constant volume spray chamber. Exp Therm Fluid Sci 2012;42:212–8. https://doi.org/10.1016/j.expthermflusci.2012.05.006.

[12] Wang X, Huang Z, Kuti OA, Zhang W, Nishida K. Experimental and analytical study on biodiesel and diesel spray characteristics under ultra-high injection pressure. Int J Heat Fluid Flow 2010;31:659–66. https://doi.org/10.1016/j.ijheatfluidflow.2010.03.006.

[13] Fu W, Li F, Meng K, Liu Y, Lin Q. Experimental and Analysis of Macroscopic Spray Characteristics of Biodiesel Blended with Di-n-butyl Ether Under Inert Conditions. Waste Biomass Valoriz 2020;11:3501–11. https://doi.org/10.1007/s12649-019-00689-8.

[14] Tran L-S, Pieper J, Zeng M, Li Y, Zhang X, Li W, et al. Influence of the biofuel isomers diethyl ether and n-butanol on flame structure and pollutant formation in premixed n-butane flames. Combust Flame 2017;175:47–59.

[15] Sarin A, Arora R, Singh NP, Sarin R, Malhotra RK, Kundu K. Effect of blends of Palm-Jatropha-Pongamia biodiesels on cloud point and pour point. Energy 2009;34:2016–21. https://doi.org/10.1016/j.energy.2009.08.017.

[16] Gao Z, Zhu L, Zou X, Liu C, Tian B, Huang Z. Soot reduction effects of dibutyl ether (DBE) addition to a biodiesel surrogate in laminar coflow diffusion flames. Proc Combust Inst 2019;37:1265–72. https://doi.org/10.1016/j.proci.2018.05.083.

[17] Fu W, Li F, Zhang H, Yi B, Liu Y, Lin Q. Liftoff behaviors and flame structure of dimethyl ether jet flame in CH4/air vitiated coflow. Proc Inst Mech Eng Part A J Power Energy 2019;233:1039–46. https://doi.org/10.1177/0957650919846007.

[18] Guan L, Tang C, Yang K, Mo J, Huang Z. Effect of di-n-butyl ether blending with soybean-biodiesel on spray and atomization characteristics in a common-rail fuel injection system. Fuel 2015;140:116–25. https://doi.org/10.1016/j.fuel.2014.09.104.

[19] Yang J, Lim O. An investigation of the spray characteristics of diesel-DME blended fuel with variation of ambient pressure in a constant volume combustion chamber. J Mech Sci Technol 2014;28:2363–8. https://doi.org/10.1007/s12206-014-0528-1.

[20] Ozkan S, Puna JF, Gomes JF, Cabrita T, Palmeira JV, Santos MT. Preliminary study on the use of biodiesel obtained from waste vegetable oils for blending with hydrotreated kerosene fossil fuel using calcium oxide (CaO) from natural waste materials as heterogeneous catalyst. Energies 2019:12. https://doi.org/10.3390/en12224306.

[21] Saxena MC, Dubey P, Tripathi A. Surface tension of binary liquid mixture. Asian J Chem 2011;23:1411–2.

[22] El-Maghraby RM. A study on bio-diesel and jet fuel blending for the production of renewable aviation fuel. Mater Sci Forum 2020;1008 MSF:231–44. 10.4028/www.scientific.net/MSF.1008.231.

[23] El-Zoheiry RM, EL-Seesy AI, Attia AMA, He Z, El-Batsh HM. Combustion and emission characteristics of Jojoba biodiesel-jet A1 mixtures applying a lean premixed pre-vaporized combustion techniques: An experimental investigation. Renew. Energy 2020;162:2227–45. https://doi.org/10.1016/j.renene.2020.10.031.

[24] Masoud SM, Attia AMA, Salem H, El-zoheiry RM. Investigation of jet A-1 and waste cooking oil biodiesel fuel blend flame characteristics stabilized by radial swirler in lean pre-vaporized premixed combustor. Energy 2023;263:125830. https://doi.org/10.1016/j.energy.2022.125830.

[25] Fernández-Sánchez ML, Fernández-Arguelles MT, Costa-Fernández JM. Atomic emission spectometry | flame photometry. 3rd ed. Elsevier Inc.; 2019. 10.1016/B978-0-12-409547-2.14533-0.

[26] Malik MSA, Mohamad Shaiful AI, Mohd Ismail MS, Mohd Jaafar MN, Sahar AM. Combustion and emission characteristics of coconut-based biodiesel in a liquid fuel burner. Energies 2017;10:1–12. https://doi.org/10.3390/en10040458.

[27] Senthur Prabu S, Asokan MA, Roy R, Francis S, Sreelekh MK. Performance, combustion and emission characteristics of diesel engine fuelled with waste cooking oil bio-diesel/diesel blends with additives. Energy 2017;122:638–48. https://doi.org/10.1016/j.energy.2017.01.119.

[28] Venu H, Madhavan V. Influence of diethyl ether (DEE) addition in ethanol-biodiesel-diesel (EBD) and methanol-biodiesel-diesel (MBD) blends in a diesel engine. Fuel 2017;189:377–90. https://doi.org/10.1016/j.fuel.2016.10.101.

[29] Lefebvre AH, Ballal DR. Gas turbine combustion: alternative fuels and emissions. CRC press; 2010.

[30] Attia AMA, Belal BY, El-Batsh HM, Moneib HA. Effect of waste cooking oil methyl ester – Jet A-1 fuel blends on emissions and combustion characteristics of a swirl-stabilized lean pre-vaporized premixed flame. Fuel 2020;267:117203. https://doi.org/10.1016/j.fuel.2020.117203.

[31] Johnson MR, Littlejohn D, Nazeer WA, Smith KO, Cheng RK. A comparison of the flowfields and emissions of high-swirl injectors and low-swirl injectors for lean premixed gas turbines. Proc Combust Inst 2005;30(2):2867–74.

[32] Carvalho M, Torres F, Ferreira V, Silva J, Martins J, Torres E. Effects of diethyl ether introduction in emissions and performance of a diesel engine fueled with

biodiesel-ethanol blends. Energies 2020;13(15):3787. https://doi.org/10.3390/en13153787.

[33] El-Zoheiry RM, EL-Seesy AI, Attia AMA, He Z, El-Batsh HM. Combustion and emission characteristics of Jojoba biodiesel-jet al mixtures applying a lean premixed pre-vaporized combustion techniques: An experimental investigation. Renew. Energy 2020;162:2227–45.

[34] Bridjesh P, Periyasamy P, Vijayarao A, Chaitanya K. MEA and DEE as additives on diesel engine using waste plastic oil diesel blends. Sustain Environ Res 2018;28: 142–7. https://doi.org/10.1016/j.serj.2018.01.001.